Balitskaya E.D.[1], Balitsky V.S.[1], Pironon J.[2], Barres O.[2], Plotnikova I.N.[3], Balitskaya L.V.[1], Golunova M.A.[1], Bublikova T.M.[1], Setkova T.V.[1]

Experimental study of the phase composition and states of water-hydrocarbon fluids at temperatures of 240–700 °C and pressures of 10–150 MPa, with the clarification of the possible maximum depths of the existence of oil in the Earth's interior

UDC 548.52+549.07+552.578.2

[1] IEM RAS, Chernogolovka (balvlad@iem.ac.ru)
[2] Université de Lorraine, Nancy
[3] IAR, TAS Kazan

Abstract. The main reason for the difference in the cracking processes of oil in an aqueous environment based on microthermometry and high-temperature FT-IR and Raman spectroscopy of synthetic water-hydrocarbon inclusions was established. Under the conditions of the predominance of an aqueous solution over oil, the oil dissolved in homogeneous, including supercritical fluids, completely loses its ability to decompose due to the formation of a true solution with water. Temperature decreasing leads to the reversible release of the same hydrocarbons and the continuation of cracking in the usual way. When oil prevails over an aqueous solution, the hydrocarbons entering into its composition, upon reaching a homogeneous state, remain as such and continue to undergo cracking and further deeper metamorphism up to irreversible transformation into methane and residual solid bitumen, up to graphite. The depths of these processes are estimated at 12 and 22 km, respectively.

Keywords: *growth of quartz, water-hydrocarbon inclusions, oil replenishment of depleted fields, oil metamorphization*

The phase composition, states and behavior of water-hydrocarbon fluids formed by the interaction of crude oil with pure water and aqueous solutions of sodium bicarbonate and sodium carbonate, sodium chloride and ammonium chloride were studied experimentally. The water-hydrocarbon interaction was carried out simultaneously with the growth of quartz crystals with fluid inclusions in the same autoclaves according to our previously developed technique (Balitsky et al., 2005; Balitsky et al., 2007; Balitsky et al., 2016; Balitsky et al., 2020). Newly formed in the experiments phases and fluid inclusions in quartz were studied using the methods of gas-liquid chromatography, normal and high-temperature local FT-IR spectroscopy, microthermometry, polarization and fluorescence microscopy. The experiments were carried out in two stages. In the first one, quartz crystals were grown in oil presence at temperatures of 240/280, 290/300, 300/330, 330/350, 350/380, 430/470, 490/500 and 680/700 °C (upper/lower autoclave zone) and pressures - from saturated steam to 150 MPa. Temperature gradient created conditions in the autoclave for the growth of quartz crystals with fluid inclusions and simultaneous the solution mixing. The grown quartz crystals were used to make polished plates 1–2 mm thick for a comprehensive study of inclusions. In the second stage, the same plates with the studied inclusions were subjected to heat treatment in pure water for two weeks at temperatures exceeding the temperature of formation of inclusions by 10–15 °C.

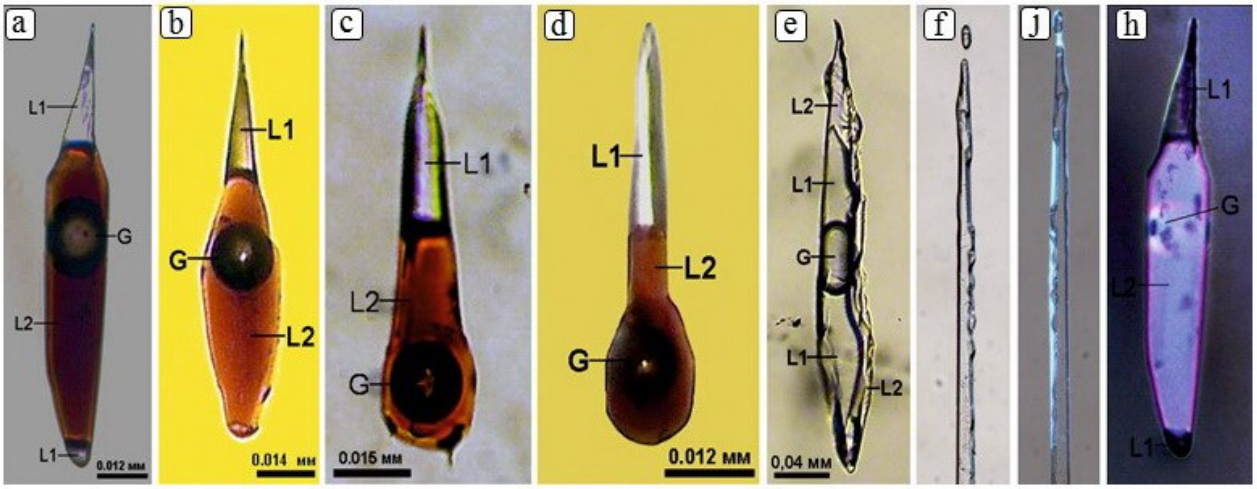

Fig. 1 Water-hydrocarbon inclusions in the overgrown layer (a, b, c, d) and seed (e, f) after autoclave heat treatment at 300 °C under day light; g, h - inclusions in ultraviolet light.

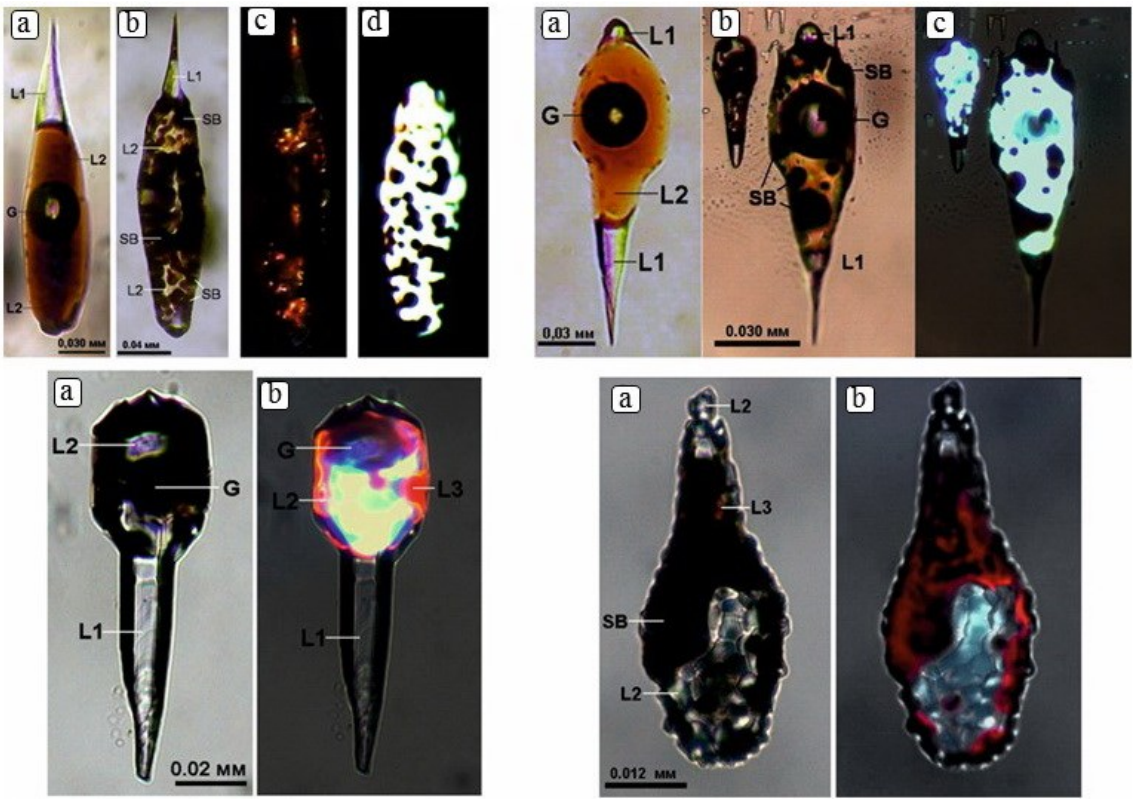

Fig.2. Upper row: primary water-oil inclusions formed at 240/280 °C (a); secondary inclusions after heat treatment at 350 °C under normal (b), polarized (c) and ultraviolet (d) light. Bottom row: secondary inclusions after heat treatment at 380 ° C under normal (a) and ultraviolet (b) light.

Pressure in the autoclaves in this case not exceed 90–100 MPa and was set according to *PVT* diagrams. This created back pressure in the autoclave, which excluded the destruction (decrepitation) of inclusions in the plates. Heat-treated inclusions were studied using the same methods that were used in the study of primary inclusions. Comparison of obtained results made it possible to clarify the effect of temperature on the metamorphic transformations of oil.

Two types of fluid inclusions were obtained resulting of growth of quartz crystals. Inclusions of the first type are located directly in the seed quartz rods. They were formed due to the mother medium penetrating into the etching channels of growth dislocations. They have exits on the basal surface of the seed rods. The inclusions are acicular, tubular, drop-shaped, and spindle-shaped and oriented in a direction close to the optical axis of the crystals. The length of the inclusions reaches 1–2 mm with a diameter of 0.005–0.02 mm. Inclusions are two- and three-phase. The volumetric ratios of the phases in them are L1> G and L1> G >> L2, where L1 - water phase, L2 - oil phase and G - gas phase (mainly water vapor). Inclusions of the second type are located in an overgrown quartz layer, located in the growth sectors of the basic pinacoid. They are also characterized by a drop-shaped and tubular shape, elongated in the direction of the optical axis, but, besides this, negative crystal and complex forms are widespread among them (Fig. 1, 2). They originated on particles of solid phases, as well as in microcavities of a rough relief, in cracks, and by fouling oil droplets that fell on the surface of the {0001} pinacoid and other faces.

The difference in phases and volumetric phase ratios indicate to heterogeneous state of the solution during the quartz growth and the capture of fluid inclusions. This affects some differences in the temperatures of partial (for example, the disappearance of only the gas phase) and complete homogenization of inclusions. At the same time, in the process of repeated short-term (0.5–1.5 hours) heating and cooling, the behavior and phase transformations in the primary inclusions are fully reproduced.

After autoclave treatment at a temperature of 300 °C for 15 days, no changes were observed in the phase composition and volumetric phase ratios in the inclusions. When they are briefly heated to 270–320 °C, a gas bubble disappears with the appearance of a liquid two-phase water-oil fluid; then, at 355–370 °C, the aqueous phase is completely dissolved in oil with the transition of the fluid to a homogeneous state. Cooling of inclusions leads to heterogenization of the fluid at 353–360 °C with its transition back to the two-phase (L1 + L2) state, followed by the appearance of a gas phase at 265–300 °C.

An increase in the temperature of autoclave treatment of inclusions to 320 °C leads to the

appearance in oil of dark brown and black semi-liquid and solid precipitates of irregular and spherical shape, as well as fine-grained aggregates having a high interference color (paraffins?) in polarized light in crossed nicols. The amount of these phases increases as autoclave treatment temperature. At the same time, the temperatures of partial and complete homogenization of the heat-treated inclusions change during their short-term heating and cooling. Changes in the composition and volumetric ratios of volatile phases in inclusions were studied by local IR spectra (Fig. 3).

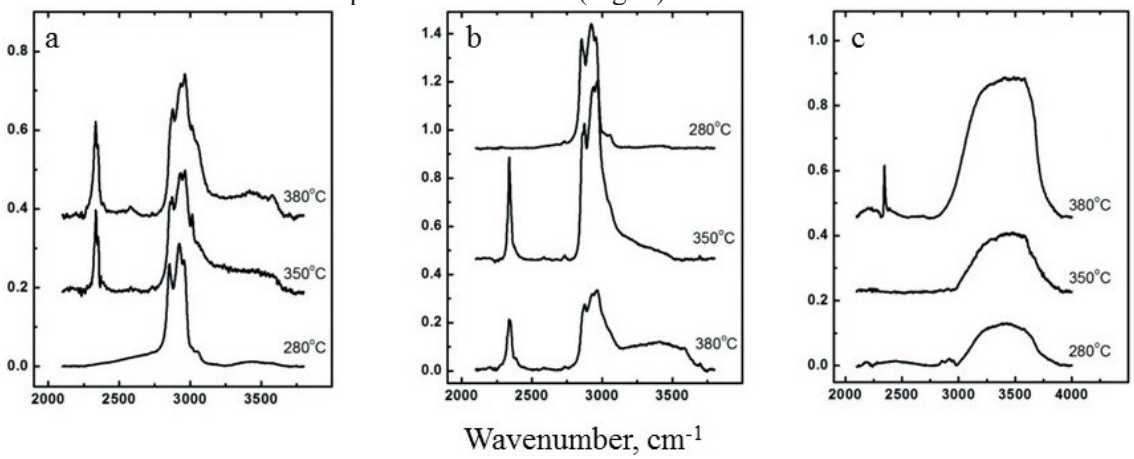

Fig.3. IR spectra of primary (280 °C) and secondary (after heat treatment at 350 and 380°C) water-oil inclusions. a – gas (mainly CH_4 and CO_2) and partially liquid hydrocarbon phases; b – liquid hydrocarbon and partly gas phases; c – water and partly gas phases.

Thus, as a result of experimental studies it was shown that oil up to temperatures of 280-300 °C retains a stable composition and do not undergoes cracking and other changes. However, at temperatures above 320 °C, oil methanization begins, accompanied by an increase in the proportion of light (gasoline, kerosene) fractions, the appearance of carbon dioxide and residual solid bitumen. At 350-380 °C this process reaches maximum intensity. It indicates the inevitable irreversible changes in oil when oil and gas deposits are immersed to deep depth and the specified temperatures are reached. The presence of solid bitumen in the rocks containing gas condensate and pure gas (methane) deposits is in good agreement with the obtained experimental data.

This study was funded by RFBR and CNRS according to the research project No 21-55-15010 and Research Program AAAA-A18-118020590150-6 of the D.S. Korzhinskii Institute of Experimental Mineralogy of Russian Academy of Sciences

References

Balitsky V.S., Balitskaya L.V., Bublikova T.M., Borkov F.P. Water-hydrocarbon inclusions in synthetic quarts, calcite, and fluorite crystals grown from oil-bearing hydrothermal solutions (experimental data) // Doklady Earth Sciences. 2005. Vol. 404. No7. P.1050–1053.

Balitsky V.S., Prokof'ev V.Yu, Balitskaya L.V., Bublikova T.M., Pentelei S.V. Experimental study of the interaction of mineral-forming hydrothermal solutions with oil and their joint migration // Petrology. 2007. Vol. 15. No 3 P. 211–223.

Balitsky V.S., Penteley S.V., Pironon J., Barres O., Balitskaya L.V., Setkova T.V. Phase states of hydrous–hydrocarbon fluids at elevated and high temperatures and pressures: Study of the forms and maximal depths of oil occurrence in the earth's interior // Doklady Earth Sciences. 2016. Vol. 466 No 2. P.130–134.

Balitsky V.S., Setkova T.V., Balitskaya L.V., Bublikova T.M., Golunova M.A. In Advances in Experimental and Genetic Mineralogy, V.11, Litvin Yu.A. Safonov O.G (Editors), New York, 2020. P. 3-34

Kovalskaya T.N.[1], Ermolaeva V.N.[1], Kalinin G.M.[1], Varlamov D.A.[1], Kovalskiy G.A.[1,2], Chaichuk K.D.[1] Synthesis of zirconium-and niobium-containing garnets under conditions of high alkalinity. Preliminary data UDC 550.4.02

[1] D.S. Korzhinsky Institute of Experimental Mineralogy RAS, Chernogolovka, Moscow district; [2] M.V. Lomonosov Moscow State University, Department of Geology, Moscow. (tatiana76@iem.ac.ru)

Keywords: *garnet, synthesis, hydrothermal conditions, alkaline pegmatites*

Under conditions of high alkalinity, zirconium and niobium can enter the anionic group, forming zirconates and niobates. Under natural conditions, these phases are confined to ultra-alkaline complexes (Khibinsky, Lovozersky, etc).

Niobates are compounds that are mixed oxides of the composition $mMxOy \cdot nNb_2O_5$, where M are atoms of one or more metals. They are subdivided into metaniobates $MNbO_3$, ortho M_3NbO_4, pyro $M_4Nb_2O_7$, poly $M_2O\ nNb_2O_5$. They are known for a lot of metals. They are close in composition and properties to numerous peroxoniobates, fluoro- and oxyfluoroniobates, chloro- and oxychloroniobates, oxide niobium bronzes [1].

Zirconates $MZrO_3$ (M - Ca, Sr, Ba) belong to the perovskite family. They have a number of valuable physicochemical and physicomechanical properties (ferroelectric, piezoelectric, etc.) [2]. According to the literature data, it is known that zirconium and niobium can be part of garnets in octahedral and tetrahedral positions [3].

Materials and methods. The experiments were carried out in platinum ampoules with a diameter of 7 mm on high pressure gas installations at p = 2.2 kbar and a temperature gradient in the reactor of 650 ° C in the upper part and 600 ° C in the lower part of the reactor. A mixture of reagents stoichiometric to the eudialyte composition was used as starting materials, and a solution of NaOH with w (NaOH) 46% was used as a fluid; the sample: fluid ratio was 15:1 by weight. The duration of the experiments was 10 days.

During the subsequent study on a Tescan Vega II XMU scanning electron microscope (Tescan, Czech Republic) equipped with an INCA Energy 450 X-ray spectral microanalysis system with energy dispersive (INCA Xsight) in the products of diagnostic experiments isometric crystals of two types of zirconium and niobium-containing garnets: with Nb_2O_5 content up to 10 wt% and ZrO_2 - 12 and 18 wt%, in which Zr and Nb are included in both octahedral and tetrahedral sites (Fig. 1).

Conclusion: Crystallization of garnets at a pressure higher than 2 kbar in alkaline conditions confirms earlier conclusions about the p-t conditions of crystallization of this mineral.

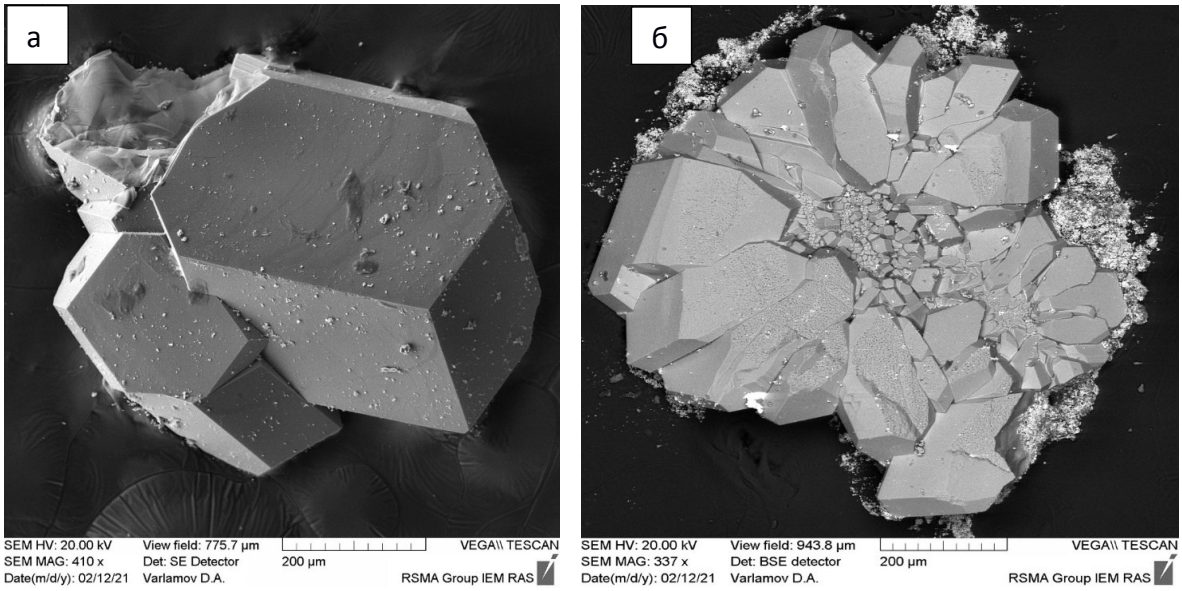

Fig. 1. Splice of garnet crystals from the experiment №0044, №0045.

Tab. 1. Chemical composition of garnets**.**

Chemical composition of granates (mas. %)														
№	1	2	3	4	5	6	7	8	9	10	11	12	13	14
Sample №	0044-	0044-0045	0044-0045	0044-0045	0044-0045	0044-0045	0044-0045	0044-0045	0045-	0045-	0045-	0045-	0045-	0045-
Analysis №	Spectrum 3	Spectrum 1	Spectrum 2	Spectrum 3	Spectrum 4	Spectrum 5	Spectrum 6	Spectrum 7	Spectrum 1	Spectrum 2	Spectrum 3	Spectrum 4	Spectrum 5	Spectrum 6
Na_2O	-	-	-	-	-	0,18	-	-	-	0,01	-	0,27	-	-
CaO	32,87	34,71	29,06	33,89	33,82	33,30	24,27	34,15	33,08	27,30	31,87	25,31	31,97	33,11
SiO_2	30,90	34,26	34,22	33,25	32,74	33,44	31,22	32,50	32,35	32,63	29,01	29,46	32,99	30,94
Fe_2O_3	29,38	31,94	24,88	33,74	33,60	33,54	23,59	33,07	31,57	23,62	30,11	23,48	24,96	27,13
TiO_2	0,02	-	-	-	0,26	-	0,23	0,17	-	0,18	0,25	-	0,20	-
ZrO_2	-	0,22	11,96	-	-	-	18,43	-	-	10,72	-	15,63	3,06	1,13
Nb_2O_5	0,83	0,56	4,39	0,55	0,36	0,19	0,81	0,03	1,53	2,73	3,67	4,01	8,83	7,89
Total	94,00	101,69	104,51	101,43	100,78	100,65	98,55	99,92	98,53	97,19	94,91	98,16	102,01	100,20

Formula coefficients (calculation for 8 cations)															
Na	-	-	-	-	-	0,03	-	-	-	-	-	0,05	-	-
Si	2,73	2,84	2,93	2,77	2,74	2,78	2,92	2,73	2,76	2,97	2,62	2,78	2,85	2,70
Ca	3,11	3,08	2,67	3,03	3,03	2,97	2,43	3,07	3,02	2,66	3,08	2,55	2,96	3,09
Ti	-	-	-	-	0,02	-	0,02	0,01	-	0,01	0,02	-	0,01	-
Fe	1,96	1,99	1,60	2,12	2,11	2,10	1,66	2,09	2,02	1,62	2,04	1,67	1,62	1,78
Zr	-	0,01	0,50	-	-	-	0,84	-	-	0,48	-	0,72	0,13	0,05
Nb	0,03	0,02	0,17	0,02	0,01	0,01	0,04	-	0,06	0,11	0,15	0,17	0,35	0,31

№	Formula
1	$Ca_{3.11}Fe_{1.96}(Si_{2.37}Nb_{0.03})_{\sum 2.39}O_{12}$
2	$Ca_{3.08}Fe_{1.99}(Si_{2.84}Nb_{0.02}Zr_{0.01})_{\sum 2.87}O_{12}$
3	$Ca_{2.67}Fe_{1.60}(Si_{2.93}Zr_{0.50}Nb_{0.17})_{\sum 3.60}O_{12}$
4	$Ca_{3.03}Fe_{2.12}(Si_{2.77}Nb_{0.02})_{\sum 2.79}O_{12}$
5	$Ca_{3.03}Fe_{2.11}(Si_{2.74}Ti_{0.02}Nb_{0.01})_{\sum 2.77}O_{12}$
6	$(Ca_{2.97}Na_{0.03})_{\sum 3.00}Fe_{2.10}(Si_{2.78}Nb_{0.01})_{\sum 2.79}O_{12}$
7	$Ca_{2.43}Fe_{1.66}(Si_{2.92}Zr_{0.84}Nb_{0.04}Ti_{0.02})_{\sum 3.82}O_{12}$
8	$Ca_{3.07}Fe_{2.09}(Si_{2.73}Ti_{0.01})_{\sum 2.74}O_{12}$
9	$Ca_{3.02}Fe_{2.02}(Si_{2.76}Nb_{0.06})_{\sum 2.82}O_{12}$
10	$Ca_{2.66}Fe_{1.62}(Si_{2.97}Zr_{0.48}Nb_{0.11}Ti_{0.01})_{\sum 3.57}O_{12}$
11	$Ca_{3.08}Fe_{2.04}(Si_{2.62}Nb_{0.15}Ti_{0.02})_{\sum 2.79}O_{12}$
12	$(Ca_{2.55}Na_{0.05})_{\sum 3.00}Fe_{1.67}(Si_{2.78}Zr_{0.72}Nb_{0.17})_{\sum 3.67}O_{12}$
13	$Ca_{2.96}Fe_{1.62}(Si_{2.85}Nb_{0.35}Zr_{0.13}Ti_{0.01})_{\sum 3.34}O_{12}$
14	$Ca_{3.09}Fe_{1.78}(Si_{2.70}Nb_{0.31}Zr_{0.05})_{\sum 3.06}O_{12}$

References

1. Sych A.M., Golub A.M. Niobates and tantalates of trivalent metals // Uspekhi khimii. 1977. T. 46. No. 3 (in russian);
2. Balyakin K.V. (2015) Synthesis of zirconates of alkaline earth metals using mechanical activation. Diss. for a job. step. Ph.D., Apatity, IKhTREMS KNTs RAN, 137 p. (in russian).
3. Edward S. Grew, Andrew J. Locock, Stuart J. Mills, Irina O. Galuskina, Evgeny V. Galuskin, Ulf Hålenius. IMA Report Nomenclature of the garnet supergroup // American Mineralogist, Volume 98, pages 785–811, 2013;

Evdokimov A. I.[1], Gurbanova O. A.[1], Antipin A.M.[2], Volkov A. S.[1], Dimitrova O. V.[1] Hydrothermal synthesis and the study of structure of a new magnesium representative of aqueous pyrophosphates family.

[1] Faculty of Geology, Lomonosov Moscow State University)
[2]-(FEDERAL RESEARCH CENTER "Crystallography and Photonics") bonik17@gmail.com, 8-985-174-7662

Abstract. The study of the crystallization of phosphates under conditions corresponding to the post-magmatic hydrothermal stage is of great interest, since it enables one to understand the processes of mineralogy and crystal-chemical features of phosphorus compounds. And also, it is interesting form the point of view of fundamental science and practical application: ortho-and pyrophosphates might have promising functional properties. A new compound (NH4)was obtained by hydrothermal synthesis at a temperature of 280 ° C and a pressure of 70 atm 2 $[(Mg)_3(P_2O_7)_2\ (H_2O)_2]$, belonging to the family of aqueous pyrophosphates with the general formula $A_2M_3(H_2O)_2[P_2O_7]_2$, where A = K, NH_4, Rb, and Na, and M = Mn, Fe, Co, and Ni. This phase was studied by X-ray diffraction analysis according to two surveys: at low (90K, nitrogen cooling) and room temperatures. The structural model in both experiments turned out to be identical, which indicates the high reliability of the data obtained. A comparative crystal chemical analysis was carried out with the minerals of pyrophosphates and orthophosphates, and with other synthetic members of this structural family.

Keywords: *hydrothermal synthesis; X-ray diffraction analysis; crystal chemistry.*

The study of the crystallization of phosphates under hydrothermal conditions is of great interest, since it gives the idea of the mineralogy and crystal-chemical features of phosphorus compounds. For a long time it was believed that only orthophosphates can be formed in nature. However, discovery of the kanafite $Na_2CaP_2O_7{\times}4H_2O$ [1] and wooldridgite $Na_2CaCu_2(P_2O_7)_2\ {\times}10H_2O$ hypergenic minerals [2], as well as the isostructured triphosphates of kanonerovite $MnNa_3P_3O_{10}{\cdot}12H_2O$ [3] and hilbronite $MgNa_3P_3O_{10}{\cdot}12H_2O$ [4] refuted this hypothesis.

A new compound $(NH_4)_2\ [(Mg)_3(P_2O_7)_2\ (H_2O)_2]$, belonging to the structural family of aqueous pyrophosphates with the general formula $A_2M_3(H_2O)_2[P_2O_7]_2$, where A = K, NH_4, Rb, and Na, and M = Mn, Fe, Co, and Ni, was obtained under hydrothermal conditions at a temperature of 280 ° C and a pressure of 70 atm. For the first time this structural type was described by Lightfoot et al. [5]. $MgCl_2$, $NH_4H_2PO_4$, and $CaCl_2$ taken in an equal mass ratio where the starting components of the system. The autoclave was kept in the oven for 20 days. An X-ray spectral chemical analysis was carried out using a JeolJSM-6480LV electron microscope equipped with an energy-dispersive X-ray spectrometer INCA Energy-350. It showed that the composition of the new compound contains Mg, N, P, and O atoms.

The X-ray diffraction studies of a single crystal of a new compound were taken at room temperature using an Xcalibur Eos S2 single-crystal diffractometer on MoKa radiation with λ= 0.71073 Å. The crystals of the new phase are monoclinic colorless prisms. A crystal with the size of 0.1 x 0.06 x 0.025 mm was selected and prepared for these experiments (Fig. 1)

The structure was modeled using the Jana 2006 software package [6], the R-factor was 2.37% and S-1.04 and was determined within the spatial group

P21/c. It consists of the layers of $[Mg_3(P_2O_7)_2(H_2O)_2]_2^{-}$, and NH^{4+} cations occupying the cavities in the interlayer space (Fig. 2).

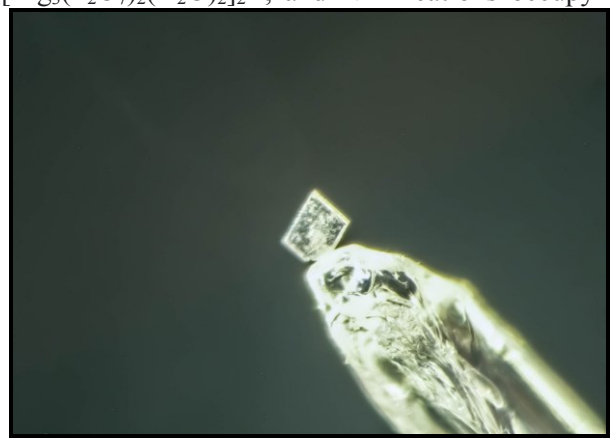

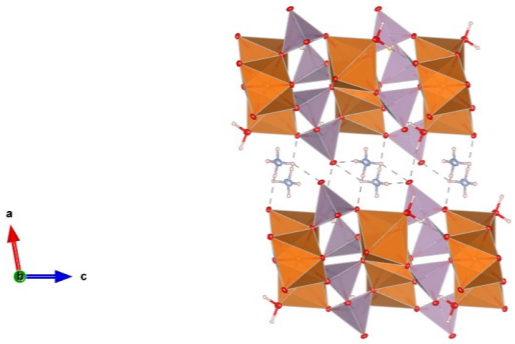

Fig. 1. The single crystals $(NH_4)_2$ $[(Mg)_3(P_2O_7)_2$ $(H_2O)_2]$, prepared for shooting on a diffractometer.

Fig. 2. The structure of $(NH4)_2[Mg_3(P_2O_7)_2$ $(H_2O)_2]$ in the projection ac. PO_4-tetrahedra is gray and MgO_6-octahedra is orange.

The new compound $(NH4)_2[Mg_3(P_2O_7)_2(H_2O)_2]$ represents the diphosphate family with the general formula $AI_2MII_3(H_2O)_2[P_2O_7]_2$, where A = K, NH_4, Rb, and Na and M = Mn, Fe, Co, Ni, and Mg. In the work by Kiryukhina [7], the dependence of the change in parameters a and b on the type of cation in positions A and M is given. The new magnesium diphosphate compound is in good correspondence with this dependence is presented.

References

Rouse R.C., Peacor D.R., Freed R.L. Pyrophosphate groups in the structure of canaphite, $CaNa_2P_2O_7 \cdot 4H_2O$; the first occurrence of a condensed phosphate as a mineral // Am. Mineral. 1988. V. 73. P. 168-171.

Cooper M.A., Hawthorne F.C. The crystal structure of wooldridgeite, $Na_2CaCu_2+2(P_2O_7)_2(H_2O)_{10}$, a novel copper pyrophosphate mineral // Can. Mineral. 1999. V. 37. P. 73-81.

Popova, V. I., Popov, V. A., Sokolova, E. V., Ferraris, G. & Chukanov, N. V. (2002): Kanonerovite, $MnNa_3P_3O_{10} \cdot 12H_2O$, first triphosphate mineral (Kazennitsa pegmatite, Middle Urals, Russia). – N. Jb. Miner. Mh. 2002 (3): 117–127; Stuttgart.

Elliott P., Brugger J., Caradoc-Davies T., Pring A. Hylbrownite, $Na_3MgP_3O_{10} \cdot 12H_2O$, a new triphosphate mineral from the Dome Rock Mine, South Australia: description and crystal structure // Mineral. Mag. 2013. V. 77(3). P. 385-398.

Lightfoot, P., Cheetham, A. K., & Sleight, A. W. // Hydrothermal synthesis and crystal structure of a new layered phosphate, $K_2Co_3(P_2O_7)_22H_2O$. // Journal of Solid State Chemistry, 1990. V.85(2). P.275–282.

Petricek, V., Eigner, V., Dusek, M. & Cejchan, A. Discontinuous modulation functions and their application for analysis of modulated structures with the computing system JANA2006 // Zeitschrift fuer Kristallographie, 2016. V.231(5). P.301-312.

Kiryukhina G. V., Crystal structures of a number of synthetic analogues of minerals with amphoteric metals, Dissertation for the degree of Candidate of Geological and mineralogical Sciences, 2016, Moscow, pp. 157-159.

K. Momma and F. Izumi, "VESTA 3 for three-dimensional visualization of crystal, volumetric and morphology data," *J. Appl. Crystallogr.*, 44, 1272-1276 (2011).

Kotelnikov A.R.[1], Suk N.I.[1], Akhmedzhanova G.M.[1], Kotelnikova Z.A.[1,2] Study of cation-exchange equilibria of solid solutions of gallium feldspars ($(Na,K)GaSi_3O_8$) with water-salt fluid UDC 550.4:549.651.1

[1]IEM RAS, Chernogolovka, Moscow district (kotelnik@iem.ac.ru); [2]IGEM RAS, Moscow (kotelnik@igem.ru)

Abstract. To obtain data on the distribution of Na and K between feldspar and solution at 550°C and 1.5 kbar under hydrothermal conditions, experimental studies of cation-exchange equilibria were carried out: $NaGaSi_3O_8$ + KCl aq = $KGaSi_3O_8$ + NaCl aq. The existence of a region of immiscibility of a solid solution is shown, the concentration dependences of the distribution coefficients of Na and K between feldspar and fluid are determined. The parameters of the unit cells of the $(Na,K)GaSi_3O_8$ solid solutions have been refined; it has been shown that the dependence of the mixing volume on the composition has an alternating character. The composition of the solid solution, at which the structural transition c1 – c2/m occurs, has been determined. On the basis of the experimental data, the calculation of the excess energies of mixing of the solid solution was carried out and the parameters of the Margules model were calculated; the correlation of the excess integrated energies and mixing volumes with the structural parameters has been carried out.

Keywords: *experiment, feldspar, unit cell parameters, solid solutions, excess mixing volumes*

Gallium alkali feldspars of the $NaGaSi_3O_8$–$KGaSi_3O_8$ series are interesting for studying the properties of minerals of the framework aluminosilicate group, as well as models of solid solutions in which structural ordering largely determines their thermodynamic properties. The aim of this study was to experimentally study the cation-exchange equilibria of gallium feldspars with a solution: $NaGaSi_3O_8$ + KCl aq = $KGaSi_3O_8$ + NaCl aq to obtain data on the distribution of Na and K between feldspar and solution, as well as to refine the parameters of the unit cells of solid solutions of synthetic gallium feldspars and estimates of excess mixing functions.

EXPERIMENTAL METHOD *Starting materials*. We used glasses $NaGaSi_3O_8$ and $KGaSi_3O_8$, obtained by melting mixtures of oxides and carbonates in a KO-14 furnace at 1250°C for 6 hours, as well as solutions of 1M NaCl + 1M KCl; ratio (sample weight)/(fluid weight) = 0.7 – 1.1. Equilibrium was approached from two sides; the duration of the experiments is 14 – 25 days.

Equipment. The experiments were carried out in hydrothermal installations with external heating and a cold seal (designed by IEM RAS) at 550°C and 1.5 kbar. The units used a water-cooled eccentric valve. The accuracy of temperature regulation and control was ± 2°C, pressure was ± 50 bar.

Analysis of the products of the experiments. The composition of the synthesized solid products of the experiments was determined using chemical analysis, as well as by the method of local X-ray spectral microanalysis using a Tescan Vega II XMU scanning electron microscope (Tescan, Czech Republic) equipped with an INCA Energy 450 X-ray spectral microanalysis system with energy dispersive (INCAx-sight) and crystal diffraction (INCA wave 700) X-ray spectrometers (Oxford Instruments, England) and the INCA Energy+ software platform. Analysis of the solution for sodium and potassium content was carried out by atomic absorption spectroscopy on a "Kvant" device.

The study of solid solutions of gallium-containing alkali feldspars was carried out on HZG-4 and Bruker diffractometers in continuous scanning mode. The refinement of the unit cell parameters was performed using the LCC, PUDI, MINCRYST programs (Burnham, 1991; Chichagov, 1994).

EXPERIMENTAL RESULTS As a result of experiments, crystals of feldspars were obtained, sometimes quartz and needle crystals of Ga_2O_3 are found in small quantities. The K-phase (K) is represented by elongated prismatic crystals; the Na-phase (N) has irregular shapes and looks like an accumulation of small gray crystallites (Fig. 1). The compositions of feldspars generally correspond to the stoichiometry of $NaGaSi_3O_8$–$KGaSi_3O_8$ solid solutions. In a number of experiments, the coexistence of phases of feldspars with different composition is observed. This indicates the presence of a region of decomposition of their solid solution. Based on the data on the compositions of the coexisting sodium and potassium phases of gallium feldspars, the boundaries of the immiscibility field of $NaGaSi_3O_8$–$KGaSi_3O_8$ solid solutions were determined. In the mole fractions of the potassium member, they correspond to $X_K^{(1)} = 0.108(51)$; $X_K^{(2)} = 0.872(62)$. The distribution of Na and K between feldspars and fluid is imperfect; in the sodium part of the system, potassium enriches the solution relative to feldspar, then an inversion occurs and, at $X_K^{Fsp} > 0.8$, potassium is redistributed to feldspar relative to the fluid. Fig. 2a shows the results of cation exchange experiments. To quantify the distribution, you can use the following expression: $K_D = [X_K^{Fsp} \times (1 - X_K^{fl})]/[(1 - X_K^{Fsp}) \times X_K^{fl}]$. Fig. 2b shows the dependence of $\ln K_D$ on the composition of gallium feldspar. This dependence is successfully described by a third degree polynomial: $\ln K_D = 3.0798 + 14.897(X_K^{Fsp}) - 20.4032(X_K^{Fsp})^2 + 11.9309(X_K^{Fsp})^3$ (±0.20).

The position of the C1↔C2/m structural transition point for gallium feldspars was estimated according to the method described in (Bambauer et al., 1984), which is based on the fact that at the C1↔C2/m transition point, the unit cell angles α and γ become equal to 90°, and accordingly, the values of the cosines of these angles become equal to 0. The following equations are obtained: (1000*cos2α) = 5.776 - 15.201*X; (1000*cos2γ) = 2.216 - 5.653*X.

Solving these equations for zero values (1000*cos2α) and (1000*cos2γ) gives the following transition point value: $X_K^{Fsp} = 0.385$ (± 0.015). These values are close to the compositions of the $Ab^h \leftrightarrow$ San transition point for the (Al, Si) – alkaline feldspar system ($X_K^{Fsp} \approx 0.45$) according to the data given in (Smith, 1974; Kroll et al., 1986, etc.).

The refinement of the parameters of the unit cells of solid solutions of gallium feldspars has been carried out. To calculate the parameters, we used the well-known unit cells parameters of end members taken from different sources as reference input data (Pentinghaus, 1980; Fleet, 1992; Kimata et al., 1995; Kotelnikov, 1995). The calculation results are shown in Fig. 3, which shows that unit cells parameters have an alternating deviation from the ideal.

To describe the solid solution of gallium alkali feldspars, we used the two-parameter Margules model, a description of which was given in (Saksena, 1975; Perchuk and Ryabchikov, 1976). This model is described by the following equation: $G^{ex} = (1-X_K^{Fsp})*(X_K^{Fsp})^2*W1 + (1-X_K^{Fsp})^2*(X_K Fsp)*W2$, where W1, W2 are the energy constants of the solid solution. The calculation of the parameters of the Margules model can be carried out in two ways: (1) on the boundaries of the solid solution decomposition

region (Perchuk, Ryabchikov, 1976; Kotelnikov, 1995); (2) from the dependence of the logarithm of the potassium distribution coefficient in the feldspar – fluid system on the composition of the solid solution using the Gibbs – Duhem equation (Orville, 1963, 1972).

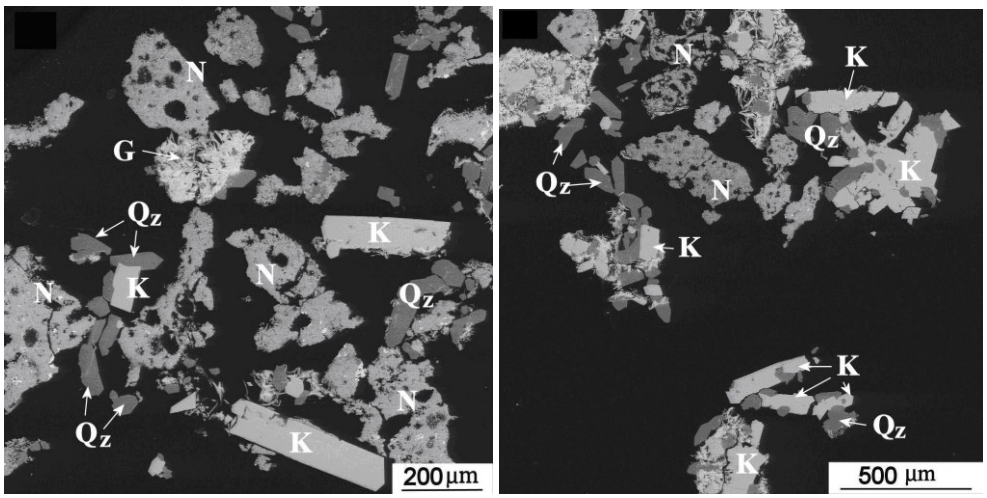

Fig. 1. Crystals of synthetic gallium feldspars. N – Na-gallium feldspars, K – K-gallium feldspars, G – Ga_2O_3, Qz – quartz.

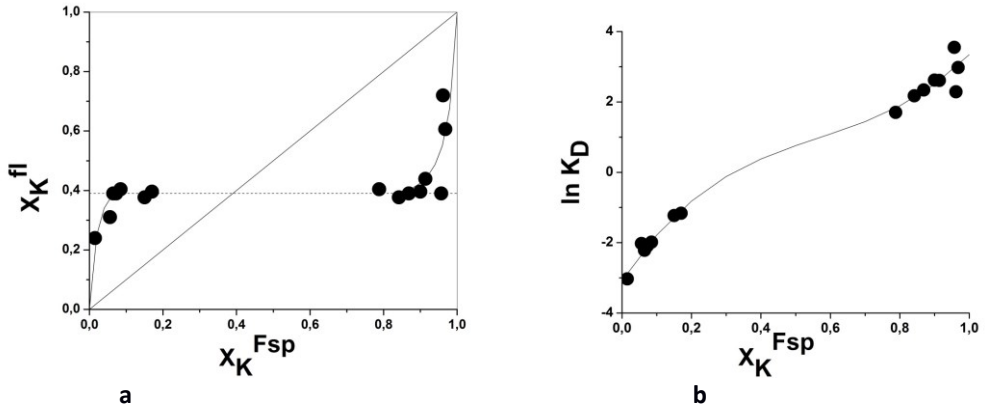

Fig. 2. Distribution of potassium and sodium between gallium alkaline feldspars and fluid (a) and the concentration dependence of the potassium distribution coefficient (lnK_D) on the composition of feldspar (b) at 550°C, 1.5 kbar.

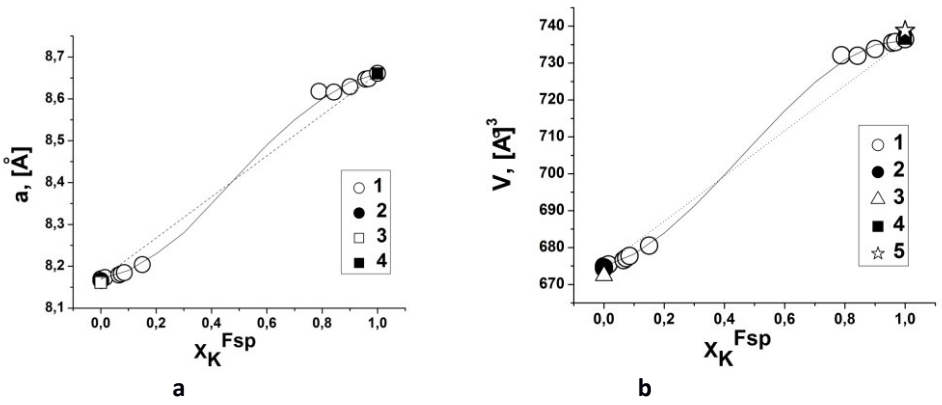

Fig. 3. Concentration dependences of the parameter a, [A] (a) and the volume of the elementary cells V, [A]3 (b).

Our data on the estimation of excess mixing functions of solid solutions of gallium alkali feldspars allow us to compare with other solid solutions of feldspars and feldspathoids. It is convenient to estimate deviations from ideal behavior using the integrated values of G^e and V^e (Kotelnikov, 1995). These values are obtained by integrating the values of the excess functions: $G^e_{int} = {}_0\int^1 G^e dX_i$; V^e_{int}

$= {}_0\int^1 V^e dX_i$; where X_i is the mole fraction of the i-th end-member of feldspars.

For comparison of solid solutions, it is convenient to use the dependences of G^e_{int} on the given dimensionless quantities A1 and A2; they are equal to A1 = (ΔR_i) (<T-O>) and A2 = (ΔR_i)/R_iT; where ΔR_i is the difference in the average radii of isomorphic cations in the frame structures of feldspars; <T-O> – values of the average distances oxygen – framework-forming cation; R_iT are the average radii of tetrahedrally coordinated cations in feldspar framework structures. G^e_{int} values versus |A1| and |A2| are described by linear regression equations (Fig. 4):

G^e_{int} = 0.3848 + 12.4270*|A1| (kJ/mol); $r_{x,y}$= 0.83, n=19, S_x = 0.75, E_x = 0.38;

G^e_{int} = 0.3120 + 3.5204*|A2| (kJ/mol); $r_{x,y}$= 0.84, n=19, S_x = 0.72, E_x = 0.36.

The dependences of the integrated excess mixing volumes on the crystal-chemical parameters A1, A2 of solid solutions of feldspars with isovalent and heterovalent types of isomorphic substitutions were determined. The relationship between V^e_{int} and the parameters A1, A2 (for isovalent type of isomorphism) is described by the following equations of the second degree (Fig. 5 a):

V^e_{int} = 0.08713 - 0.392059*(A1) + 6.230197*$(A1)^2$; n=8, S_x=0.09, E_x=0.07

V^e_{int} = 0.05693 + 0.10277*(A2) + 0.33053*$(A2)^2$; n=8, S_x=0.17, E_x=0.12.

For systems of solid solutions with a heterovalent type of isomorphism (the V^e_{int} values can have negative values), the relationship between the integrated mixing volumes and the parameters A1 and A2 is well described by the equations of the second degree (Fig. 5b):

V^e_{int} = 0.0270 + 4.766*A1 + 10.3706*$(A1)^2$; n=7; S_x = 0.15; E_x = 0.12;

V^e_{int} = 0.0273 + 1.2821*A1 + 0.75080*$(A1)^2$; n=7; S_x = 0.14; E_x = 0.12.

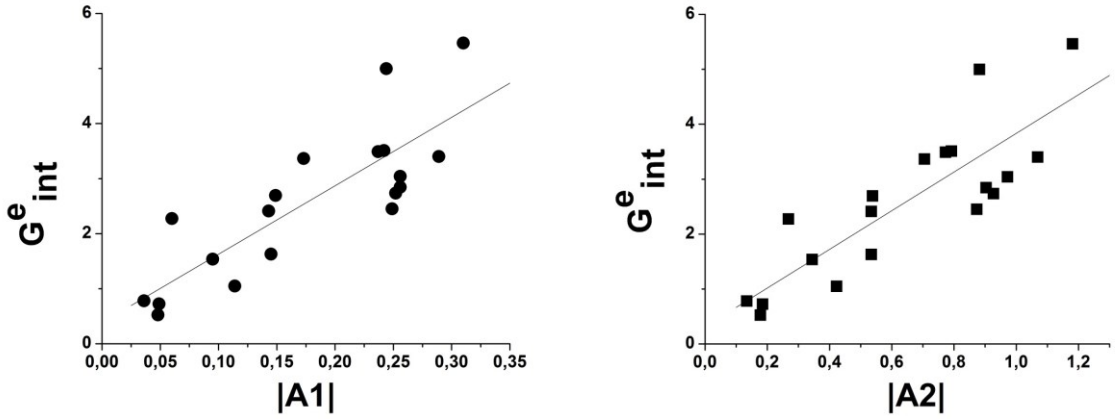

Fig. 4. Dependences of the integrated energies of mixing of solid solutions of feldspars on the parameters A1, A2.

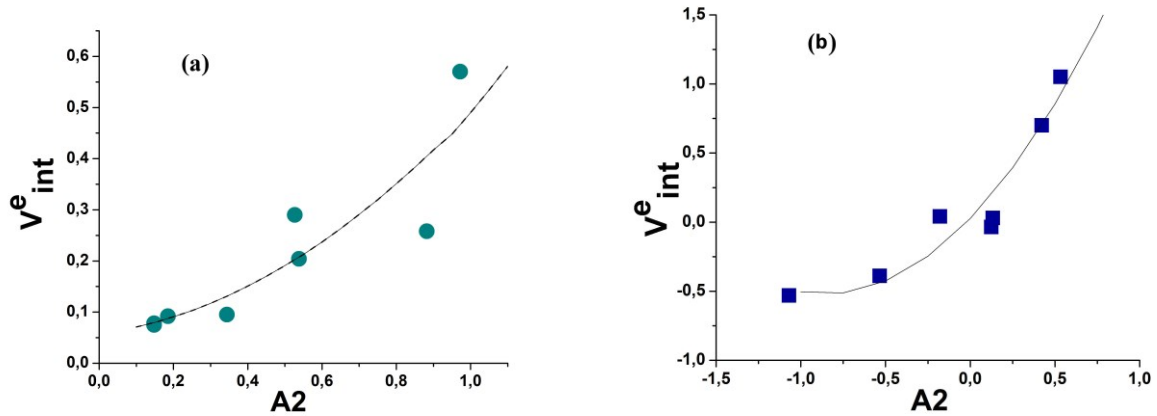

Fig. 5. Dependence of the integrated mixing volumes on the crystal-chemical parameter A2 for systems with isovalent type of isomorphic substitutions (a) and for systems with heterovalent type of isomorphic substitutions (b).

This work was supported by the AAAA-A18-118020590150-6 program.

References

Kotelnikov A.R. Isomorphism in framework aluminosilicates. Abstract dissertation. doct. geol-min. sciences. Moscow: Moscow State University, 1995. 36 p.

Perchuk L.L., Ryabchikov I.D. Phase correspondence in mineral systems. Moscow: Nedra, 1976. 287 p.

Saxena S. Thermodynamics of solid solutions of rock-forming minerals. M .: Mir. 1975. 208 p.

Bambauer H.U., Schops M., Pentinghaus H. Feldspar phase relations in the system $NaAlSi_3O_8$–$SrAl_2Si_2O_8$ // Bull. Mineral. 1984. V. 107. P. 541–551.

Burnham C.W. Least-squares refinement of crystallographic lattice parameters for IBM PC/XT/AT and compatibles. Cambridge: Harvard University, 1991. (Program Description, 24 p.).

Chichagov A.V. Information-calculating system on crystal structure data of minerals (MYNCRYST) // Materials Science Forum, vols. 166–169. Trans Tech Publications. Switzerland. 1994. P. 187–192.

Fleet M.E. Structures of low gallium albite ($NaGaSi_3O_8$) and intermediate germanium albite ($NaAlGe_3O_8$): tetrahedral-site ordering in sodium feldspar // Amer. Mineral. 1992. V. 77. P. 76–84.

Kimata M., Saito S., Shimizu M. Structure of sanidine type $KGaSi_3O_8$ tetrahedral-site disordering in potassium feldspar // Eur. J. Mineral. 1995. V.7. P. 287–296.

Kroll H., Schmiemann I., von Colln G. Feldspar solid solutions //Amer. Mineral. 1986. V.71. P.1–16.

Orville P.M. Alkali ion exchange between vapor and feldspar phases//Amer. J. Sci. 1963. V. 261. P.201–237.

Orville P.M. Plagioclase cation exchange equilibria with aqueous chloride solution: results at 700°C and 2000 bars // Amer. J. Sci. 1972. V. 272. № 3. P. 234–273.

Pentinghaus H. Polimorphie in den feldspatbildenden systemen A+T3+T4+O8 und A2+T23+T24+O8 alkali-und erdalkali-, bor-, aluminium-, gallium-, eisen-silicate und –germanate//Habil. Diss. Munster. 1980. 210 p.

Setkova T.V. [1], Balitsky V.S. [1], Spivak A.V. [1], Iskrina A.V. [1,2], Kuzmin A.V. [3], Bublikova T.M.[1], Khasanov S.S. [1,3] Hydrothermal synthesis and structure of brunogeierite (Fe_2GeO_4)

UDC 549.731.11

[1] IEM RAS (Chernogolovka), [2] Lomonosov MSU (Moscow), [3] ISSP RAS (Chernogolovka)
setkova@iem.ac.ru

Abstract. Brunogeierite crystals $(Fe^{2+})_2Ge^{4+}O_4$ up to 500 μm in size were obtained in autoclave at a temperature of 600/650 °C and a pressure of 100 MPa as a result of the interaction of a boric acid solution on a metal iron wire in the presence of germanium oxide (GeO_2). Synthetic brunogeierite crystallizes in the space group *Fd3m*, has a spinel structure with unit cell parameters: a = 8.3783(6) Å, V = 588.12(13) Å^3.

Keywords: *brunogeierite, spinel, synthesis, structure, hydrothermal solutions*

Introduction. The rare Ge-mineral brunogeierite with a spinel structure was found first in the lower oxidation zone of the hydrothermal polymetallic ore deposit of the Tsumeb deposit, Namibia (Otteman and Nuber 1972). Later brunogeierite was found in several other locations in the French Pyrenees (Johan and Oudin 1986, Höll et al., (2007). Natural crystals were small, sufficient only to determine some structural characteristics (Welch et al., 2001). Brunogeierite belonging to spinel structural type opens up the possibility of using it in various fields of technology. For example, nanosized crystals of $(Fe)_2GeO_4$ find application in technologies for creating materials for lithium and sodium-ion batteries (Han et al., 2018). In addition, germanates are often used as structural analogs of high-pressure silicates, since they allow to study phase transformations and structural behavior at pressures, which are more accessible experimentally than for the corresponding silicate systems. The obtaining of synthetic brunogeierite crystals of sufficient size to determination the physical properties is actual direction for sciences and technology.

Methods. The synthesis of brunogeierite crystals was carried out under thermo-gradient hydrothermal conditions at temperature of 600-650 °C and pressure of 100 MPa in autoclaves made of Cr-Ni alloy. Platinum-lined inserts with an internal volume of 5 ml were used (Fig. 1). Iron wire and germanium oxide were used as nutrient material; their ratio was 2:1 and calculated from brunogeierite stoichiometry. The wire was located along the insert length, germanium oxide at the bottom. A solution of 30 wt% boric acid was poured into the inserts loaded with a nutrient. The ratio of the solid phases and solution was 1:1. The inserts were hermetically sealed, weighed and placed in an autoclave containing three inserts at a time. Next, the autoclave was heated in an electric furnace up to temperature of 650 (lower part) and 600 °C (upper part). Pressure was set by the filling factor of the insert and autoclave and was estimated from *P-V-T* diagrams for pure water (Wagner and Pruss 2002). Duration of experiments was 20 days. The experimental products were studied by optical (MBS-10, ADF), polarizing (Nikon Eclipse LV100pol), and scanning electron (Tescan Vega II XMU) microscopes. The compositions of the new formed crystals were determined using electron probe microanalysis (Tescan Vega II XMU). The structural characteristics were refined on a Rigaku Oxford Di raction "Gemini R" CCD with MoKα (λ = 0.71073 Å).

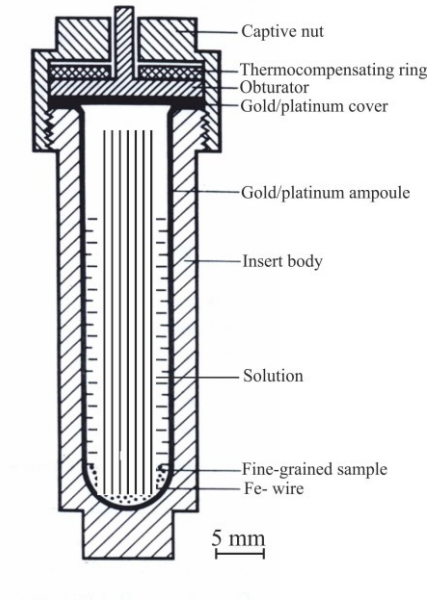

Fig. 1. Scheme of insert filling in experiments on the brunogeierite synthesis

Results. Crystals of brunogeierite with size of 50 to 500 μm of dark brown color were obtained. Crystals were formed mainly on the surface of the iron wire (Fig. 2a). The largest ones crystallize in the upper growth zone, where supersaturation with respect to germanium oxide is higher. The crystals habit is mainly composed of the faces of the {111} octahedron, with a wide development of twinning according to the spinel law, less often faces of the rhombic dodecahedron {110} are present (Fig. 2b).

Synthetic brunogeierite crystallizes in the space group *Fd3m* with lattice parameters a = 8.3783 (6) Å; V = 5.608 Å3; Z = 8 (Tables 1-2). The oxides of spinel family exhibit the general formula AB_2O_4, where the B cation coordinates in edge-sharing octahedra and the A cation occupies tetrahedra. The refined site occupancies indicate that Ge and Fe are fully ordered at the A and B sites, respectively, i.e. Fe_2GeO_4 is a normal spinel (Welch et al., 2001). So, our brunogeierite has a normal spinel structure with eighth formula units $[^{VI}(Fe^{2+})_2{}^{IV}(Ge^{4+})O_4]$ in a primitive unit cell. The normal spinel structure consists of a cubic close-packed array of oxygen atoms with divalent cations $^{VI}(Fe^{2+})$ occupying half of the octahedral interstices and tetravalent cations $^{IV}(Ge^{4+})$ occupying one eighth of the tetrahedral interstices.

In the structure of the synthetic brunogeierite crystal the bond distances of Ge –O is 1.782(10) Å and Fe – O is 2.113(6) Å. The bond distances of a synthetic crystal are slightly differ than the theoretical ones, which should be equal to the sum of the ionic radii. The Ge – O and Fe –O bond lengths are 0.39+1.38=1.77 Å and 0.78+1.38=2.16 Å, respectively. At the same time, the data obtained earlier on the distance of bonds in a natural sample brunogeierite showed the correspondence to calculated (Welch et al., 2001).

Conclusions. Brunogeierite crystals with a spinel structure were obtained for the first time at hydrothermal conditions (temperature 600/650 °C and pressure 100 MPa) as a result of the interaction of boric acid solution with iron wire in presence of hexagonal germanium oxide. The refined structural characteristics of the obtained crystals are in agreement with the data for natural and synthetic polycrystalline brunogeierite (Welch et al., 2001, Strobel et al., 1980). The size and quantity of crystals allows carrying out additional studies of the physical properties of synthetic brunogeierite, which is planned in the future.

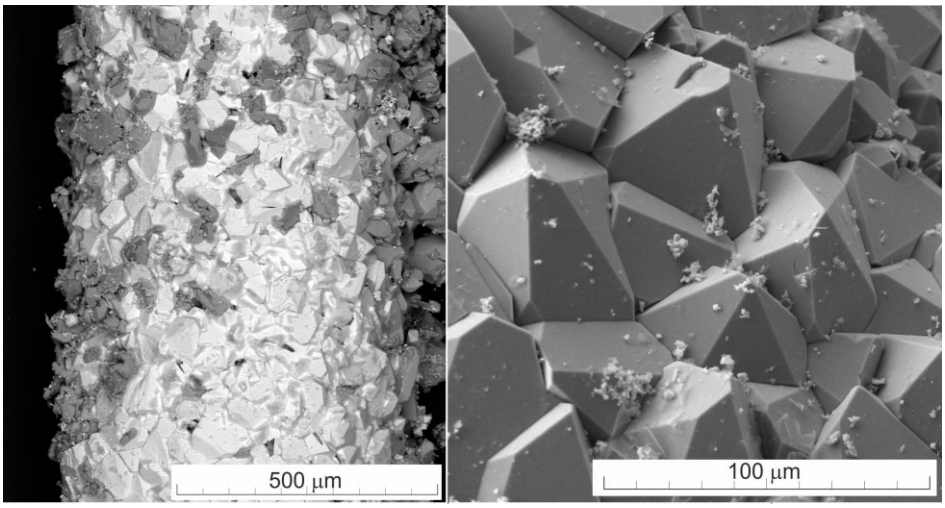

Fig. 2. Brunogeierite crystals formed on surface of iron wire (a) in boric acid solution at 600/650 °C and 100 MPa, enlarged image (b).

Table 1. Crystallographic characteristics, details of the X-ray experiment, and structure refined parameters for brunogeierite Fe_2GeO_4.

Formula weight	248.29
Space group	*Fd3m*
a, b, c, Å	8.3783(6), 8.3783(6), 8.3783(6)
V, Å3	588.12(13)
Z	8
F(000)	928
ρ, g/cm3	5.608
Radiation sours type	MoKα, 0.71073
T, (K)	258(20)
Crystal size, μm	112x69x49
Diffractometer	Rigaku Oxford Diffraction "Gemini R" CCD
Θmin - Θmax, град	6.9-32.4
h, k, l ranges	$-21 \le h \le 10$, $-11 \le k \le 9$, $-12 \le l \le 12$
Rint	0.0543
GooF	1.152

Table 2. Structural data for brunogeierite

Sample	a(Å)	V(Å3)	Cell content (Z)	Density	References
Natural (Tsumed, Namibia)	8.4127(7)	595.4(1)	8	n.d.	Welch et al., 2001
Synthetic polycrystalline	8.4118	595.2	8	Calc. 5.54 Meas. 5.51	Strobel et al., 1980
Synthetic single crystal	8.3783(6)	588.12(13)	8	5.608	This study

n.d. – no data

This work is fulfilled under the Research Programs AAAA-A18-118020590140-7 and AAAA-A18-118020590150-6 of the Korzhinskii Institute of Experimental Mineralogy RAS.

References

Höll R, Kling M, Schroll E, Metallogenesis of germanium – a review. Ore Geol Rev 30 (2007): 145–180

Jinzhi Han, Jian Qin, Lichao Guo, Kaiqiang Qin, Naiqin Zhaoa, Chunsheng Shi, Enzuo Liua, Fang He, Liying Ma, Chunnian He, Ultrasmall Fe2GeO4 nanodots anchored on interconnected carbon nanosheets as high-performance anode materials for lithium and sodium ion batteries. Applied Surface Science 427 (2018): 670–679

Johan Z, Oudin E, Présence de grenats,$Ca_3Ga_2(GeO_4)_3$, $Ca_3Al_2[(Ge,Si)O_4]_3$ et dun equivalent ferrifère, germanifère et gallifère de la sapphirine, $Fe_4(Ga,Sn,Fe)_4(Ga,Ge)_6O_{20}$, dans la blende des gisements de la zone axiale pyrénéenne. Conditions de formation des phases germanifères et gallifères. C R Acad Sci Paris Série II 303 (1986): 811–816

Ottemann J, Nuber B, Brunogeierit, ein Germanium Ferritspinell von Tsumeb. Neu Jb Mineral, Mh (1972): 263–267

Strobel P, Koffyberg F P, Wold Aa, Electrical and Optical Properties of High-Purity p-Type Single Crystals of $GeFe_2O_4$, J. Solid State Chem. 31 (1980): 209–216.

Wagner W., Pruss A. J. Phys. Chem. Ref. Data. 31 (2) (2002) : 387.

Welch MD, Cooper MA, Hawthorne FC, The crystal structure of brunogeierite, Fe2GeO spinel. Mineral Mag 65 (2001): 441–444

Kovalskaya T.N.[1], Ermolaeva V.N.[1], Varlamov D.A.[1], Kalinin G.M.[1], Kovalskiy G.A.[1,2], Chaichuk K.D.[1] Hydrothermal synthesis of eudialite phases UDC 550.4.02

[1] D.S. Korzhinsky Institute of Experimental Mineralogy RAS, Chernogolovka, Moscow district;
[2] M.V. Lomonosov Moscow State University, Department of Geology, Moscow.
(tatiana76@iem.ac.ru)

Abstract: This work is devoted to the synthesis of eudialite and the possibility of entering into its structure Nb, Ti, La, Sr with the formation of eudialite-like phases. Experiments on the synthesis of eudialite were carried out in platinum ampoules with a diameter of 4-5 mm on high-pressure gas installations at a temperature of 550-650°C

and a pressure of 1.8-2.0 kbar in accordance with the assumed physic-chemical conditions for the formation of pegmatites of the Lovozero and Khibiny massifs.

***Keywords**: eudialite, synthesis, hydrothermal conditions, alkaline pegmatites*

The process of metal cations separation from eudialyte and its decomposition has been sufficiently studied and described just now (Smirnova et al., 2015; Smirnova et al., 2015). However, synthesis of eudialite is a problem, due to the low knowledge of the conditions of its formation, and is an urgent task for experimental mineralogy.

Eudialite is a ring sodium, calcium, zirconosilicate with the ideal formula – $Na_{15}Ca_6Fe^{2+}3Zr_3(Si_{26}O_{73})(O,OH,H_2O)_3(Cl,OH)_2$ (Rastsvetaeva et al., 2020). Composition of eudialite may contain impurities Nb, Ta, REE, S, Y, etc. The crystal structure of eudialite is extremely complex, since there are two types of rings made of silicon-oxygen tetrahedra: ternary and ninefold. It is found only among igneous alkaline rocks (nepheline syenites) and in pegmatite separations in paragenesis with nepheline, feldspar, etc. in ultra-alkaline massifs (Lovozersky, Khibinsky, etc.) (Yakovenchuk et al., 1999). There are known rocks with such a significant distribution of eudialite that it becomes a rock-forming one, for example, eudialite luyavrite. Large deposits are located in the Khibinsky and Lovozersky alkaline massifs (Kola Peninsula). There are also deposits in Canada, the United States, Greenland and Norway.

The studied samples were synthesized from stoichiometric simplified gels of eudialyte composition using the following reagents: CaO, Fe_2O_3, $ZrOCl_2*8H_2O$, Nb_2O_5 and amorphous SiO_2. Sodium was introduced into the system through an aqueous solution of NaOH (46 wt.%) in the volume corresponding to the stechiometric amount of sodium to the mass of the gel based on the eudialite formula, which corresponds to the ultra-alkaline conditions of eudialite formation. Fluid (1M NaCl) was also added to the system in a weight/fluid ratio of 10/1 by weight. As a seed material was used natural eudialyte of the Lovozero massif (pegmatite of the northern quarry of the Umbozero mine) in the amount of 1% of the mass of the initial reaction mixture and fluids. Naturale seed material of eudialite has composition: $(Na_{14.03}K_{0.24})_{14.27}Ca_{3.34}(Fe^{2+}_{2.30}Mn_{0.60})_{2.90}(Zr_{3.23}Ti_{0.24})_{3.47}(Si_{0.81}Nb_{0.19})(Si_{25}O_{73})Cl_{1.08}S_{0.12}$.

The experiments were carried out in platinum ampoules with a diameter of 4 and 5 mm on high-pressure gas installations, at temperature conditions: 600-550°C and 650-600°C (bottom-top of ampoules with a reaction mixture), and at a pressure of 1.8 and 2.0 kbar, respectively, which is comparable with the assumed physico-chemical conditions for the formation of pegmatites of the Lovozersky and Khibinsky massifs (Ageeva et al., 2002; Pekov, 2004). Duration of experiments was 10 days.

As a result of the experiments, beige-green crystal aggregates up to 40 microns were obtained (Fig. 1). During a detailed microscopic study using a scanning electron microscope Tescan Vega II XMU (Tescan, Czech Republic), equipped with an INCA Energy 450 X-ray spectral microanalysis system with energy dispersion (INCA Xsight) and crystal diffraction (INCA wave 700) X-ray spectrometers (Oxford Instruments, England) and the INCA Energy+ software platform, as well as during the decoding of X-ray phase analysis spectra in experiments where as a fluid a 1M NaCl solution was used, at P-T parameters: 600-550°C / 1.8 kbar, a typical association of alkaline pegmatites was found - aegirine + elpidite + eudialyte (composition: $Na_{15}Ca_6(Fe^{2+},Mn^{2+})_3(Zr,Nb)_3[Si_{25}O_{73}](O,OH,H_2O)_3(Cl,OH)_2$ (Table. 1)) + petrazite, corresponding to the pegmatites of the Lovozersky massif.

The data obtained in the course of the work showed that the newly formed eudialyte is different in composition from the original one (naturale seed of eudialite), and that during crystallization, niobium enters its structure, and the new eudialyte is enriched in cerium, titanium, lanthanum and strontium, the migration of which, from the seed, is probably due to an increase in their mobility in the alkaline fluid medium.

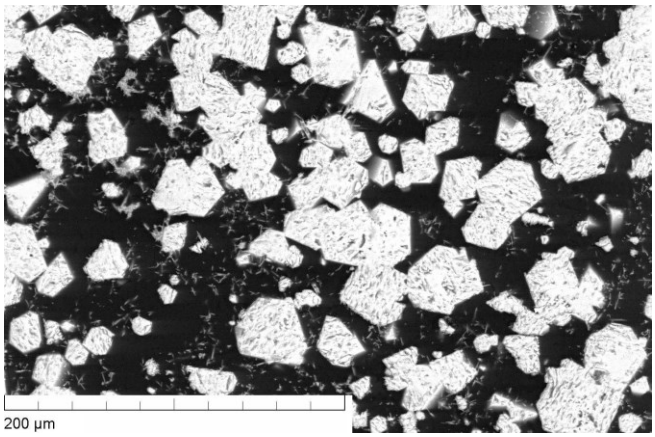

Figure 1. Crystals of synthesized eudialite (Sample with NaCl + NaOH).

Table 1. Chemical composition (wt. %) of natural and synthetic eudialytes.

	Sample with NaCl + NaOH		Sample with NaOH	
components	Seed of eudialite	Synthesized eudialite	Seed of eudialite	Synthesized eudialite
SiO_2	53.56	49.91	53.81	51.02
ZrO_2	18.59	14.12	17.43	14.89
TiO_2	0.07	0.05	0.1	0.08
Al_2O_3	0.24	0.09	0.19	0.15
Fe_2O_3	0.28	1.61	0.25	1.18
CaO	15.41	17.41	15.01	16.23
Na_2O	7.84	11.50	7.73	11.17
SrO	0.79	0.49	0.75	0.55
Nb_2O_5	0.82	2.57	2.80	3.68
La_2O_3	0.25	0.15	0.23	0.11
Ce_2O_3	0.25	0.19	0.20	0.13
Cl	1.8	1.05	1.16	0.65
Total	99.2	98.75	97.6	99.83

References

Ageeva O.A., Borutskiy B.E., Khangulov V.V. Eudialyte as a mineralogical-geochemical indicator of metasomatic processes during the formation of rocks of the poikilitic nepheline syenite complex of the Khibiny massif. - Geochemistry. 2002. No. 10. S. 1098-1105.

Pekov I.V., Podlesniy A.S. Mineralogy of the Kukisvumchorr deposit (alkaline pegmatites and hydrothermalites). - Moscow. Association Ecost, Mineralogical Almanac, vol. 7, 2004 .-- 176 p.

Rastsvetaeva R.K., Chukanov N.V., I.V. Pekov, Christof Schäfer, K.V. Van New Data on the Isomorphism in Eudialyte-Group Minerals. 1. Crystal Chemistry of Eudialyte-Group Members with Na Incorporated into the Framework as a Marker of Hyperagpaitic Conditions // Minerals 2020, 10, 587, pp. 2-16.

Smirnova T. N., Pekov I. V., Varlamov D. A., Kovalskaya T. N., Bychkov A. Y., and Bychkova Y. V. Specific features of eudialyte decomposition in oxalic acid. In Alkaline Magmatism of the Earth and Related Strategic Metal Deposits Proceedings of XXXII International Conference (2015), pp. 119– 121.

Smirnova T.N., Pekov I.V., Varlamov D.A., Kovalskaya T.N., Bychkov A.Y., Bychkova Y.V. About the chemistry and stages of phase processes during acid decomposition of eudialyte (according to experimental data). In Ontogeny, phylogeny, system of mineralogy. Materials of the All-Russian Conference, Miass, 2015, pp. 167-170, (in russian).

Yakovenchuk V.N., Ivanuk G.Y., Pakhomovskiy Y.A., Menshikov Y.P. Minerals of the Khibiny massif. - Moscow. Ed. "Earth", 1999. 326 p, (in russian).